Ore Geology Reviews 68 (2015) 171–194

Contents lists available at ScienceDirect

Ore Geology Reviews

journal homepage: www.elsevier.com/locate/oregeorev

Fluid types and their genetic meaning for the BIF-hosted iron ores, Krivoy Rog, Ukraine

Marta Sośnicka [a,b,*], Ronald J. Bakker [c], Curt Broman [d], Iain Pitcairn [d], Ihor Paranko [e], Kingsley Burlinson [f]

[a] AGH University of Science and Technology, Faculty of Geology, Geophysics and Environmental Protection, Department of Economic Geology, al. A. Mickiewicza 30, 30-059 Krakow, Poland
[b] Economic Geology Research Institute, School of Geosciences, University of the Witwatersrand, Private Bag 3, 2050 Wits, Johannesburg, South Africa
[c] Resource Mineralogy, Department of Applied Geosciences and Geophysics, Montanuniversitaet Leoben, Peter-Tunner-Str. 5, 8700 Leoben, Austria
[d] Department of Geological Sciences, Stockholm University, 10691 Stockholm, Sweden
[e] Kryvorizkiy National University, Kryvyj Rig, XXII Partzyizdu Str., 11, 50027 Krivoy Rog, Ukraine
[f] Burlinson Geochemical Services Pty. Ltd., Darwin, NT, Australia

ARTICLE INFO

Article history:
Received 14 May 2014
Received in revised form 25 November 2014
Accepted 4 December 2014
Available online 9 January 2015

Keywords:
Banded iron formation
BIF
Fluid inclusions
High-grade iron ore
Ore genesis
Krivoy Rog
Kryvyj Rig

ABSTRACT

This paper contributes to the understanding of the genesis of epigenetic, hypogene BIF-hosted iron deposits situated in the eastern part of Ukrainian Shield. It presents new data from the Krivoy Rog iron mining district (Skelevatske–Magnetitove deposit, Frunze underground mine and Balka Severnaya Krasnaya outcrop) and focuses on the investigation of ore genesis through application of fluid inclusion petrography, microthermometry, Raman spectroscopy and baro-acoustic decrepitation of fluid inclusions. The study investigates inclusions preserved in quartz and magnetite associated with the low-grade iron ores (31–37% Fe) and iron-rich quartzites (38–45% Fe) of the Saksaganskaya Suite, as well as magnetite from the locally named high-grade iron ores (52–56% Fe). These high-grade ores resulted from alteration of iron quartzites in the Saksaganskiy thrust footwall (Saksaganskiy tectonic block) and were a precursor to supergene martite, high-grade ores (60–70% Fe). Based on the new data two stages of iron ore formation (metamorphic and metasomatic) are proposed.

The metamorphic stage, resulting in formation of quartz veins within the low-grade iron ore and iron-rich quartzites, involved fluids of four different compositions: CO_2-rich, H_2O, H_2O–CO_2($\pm N_2$–CH_4)–NaCl($\pm NaHCO_3$) and H_2O–CO_2($\pm N_2$–CH_4)–NaCl. The salinities of these fluids were relatively low (up to 7 mass% NaCl equiv.) as these fluids were derived from dehydration and decarbonation of the BIF rocks, however the origin of the nahcolite ($NaHCO_3$) remains unresolved. The minimum P–T conditions for the formation of these veins, inferred from microthermometry are $T_{min} = 219$–246 °C and $P_{min} = 130$–158 MPa. The baro-acoustic decrepitation analyses of magnetite bands indicated that the low-grade iron ore from the Skelevatske–Magnetitove deposit was metamorphosed at T = ~530 °C.

The metasomatic stage post-dated and partially overlapped the metamorphic stage and led to the upgrade of iron quartzites to the high-grade iron ores. The genesis of these ores, which are located in the Saksaganskiy tectonic block (Saksaganskiy ore field), and the factors controlling iron ore-forming processes are highly controversial. According to the study of quartz-hosted fluid inclusions from the thrust zone the metasomatic stage involved at least three different episodes of the fluid flow, simultaneous with thrusting and deformation. During the 1st episode three types of fluids were introduced: CO_2–CH_4–N_2($\pm$C), CO_2($\pm N_2$–CH_4) and low salinity H_2O–N_2–CH_4–NaCl (6.38–7.1 mass% NaCl equiv.). The 2nd episode included expulsion of the aqueous fluids H_2O–N_2–CH_4–NaCl($\pm CO_2$, $\pm$C) of moderate salinities (15.22–16.76 mass% NaCl equiv.), whereas the 3rd event involved high salinity fluids H_2O–NaCl($\pm$C) (20–35 mass% NaCl equiv.). The fluids most probably interacted with country rocks (e.g. schists) supplying them with CH_4 and N_2. The high salinity fluids were most likely either magmatic–hydrothermal fluids derived from the Saksaganskiy igneous body or heated basinal brines, and they may have caused pervasive leaching of Fe from metavolcanic and/or the BIF rocks. The baro-acoustic decrepitation analyses of magnetite comprising the high-grade iron ore showed formation T = ~430–500 °C. The fluid inclusion data suggest that the upgrade to high-grade Fe ores might be a result of the Krivoy Rog BIF alteration by multiple flows of structurally controlled, metamorphic and magmatic–hydrothermal fluids or heated basinal brines.

* Corresponding author at: Economic Geology Research Institute EGRI, School of Geosciences, University of the Witwatersrand, Private Bag 3, 2050 Wits, Johannesburg, South Africa.
E-mail address: sosnickamarta@gmail.com (M. Sośnicka).

http://dx.doi.org/10.1016/j.oregeorev.2014.12.022

1. Introduction

Iron ore deposits within Precambrian banded iron formations (BIFs) are the most profitable sources of iron making them very attractive exploration targets (Duuring et al., 2012). However there are many aspects of their genesis and evolution that are controversial and not fully understood, not least the mechanisms of iron ore enrichment, which have been a subject of recent intense research (e.g. Rosière and Rios, 2004; Hagemann et al., 2006; Belykh et al., 2007; Beukes et al., 2008; Spier et al., 2008; Thorne et al., 2009; Angerer et al., 2012; Figueiredo e Silva et al., 2013).

Recently improved genetic models for Fe deposits hosted by BIFs worldwide, e.g. Kursk Group, KMA, Russia (~2.39 Ga), Brockman Iron Formation, Hamersley Basin, Australia (~2.46 Ga), itabirites of the Cauê Formation, Brazil (~2.45 Ga) or Serra Norte Carajás BIF, Brazil (~2.7 Ga) are primarily focused on a direct transition from a BIF-protolith to the high-grade (>58% Fe) martite and hematite ores (e.g. Belykh et al., 2007; Spier et al., 2008; Thorne et al., 2009; Figueiredo e Silva et al., 2013). According to these models the ore-forming fluids, interacting with the BIF-protolith, played a crucial role in the iron ore enrichment (Belykh et al., 2007; Spier et al., 2008; Thorne et al., 2009; Figueiredo e Silva et al., 2013). For instance, martite and specular hematite–martite, high-grade ores from Fe deposits of the KMA region, which are hosted by BIF similar in age and tectonostratigraphic setting to the Krivoy Rog BIF, were upgraded during the introduction of meteoric waters and unknown hypogene fluids derived from deep-seated sources (Belykh et al., 2007). The most recent fluid flow models worldwide also propose multiple interactions of BIF with fluids of various origins, e.g. hypogene and supergene meteoric fluids in Fe deposits of the Quadrilátero Ferrífero region, Brazil (Spier et al., 2008), supergene and modified hydrothermal fluids in deposits of the Iron Ore Group, India (Beukes et al., 2008), basinal brines and meteoric fluids in Hamersley-type deposits, Australia (Hagemann et al., 2006; Thorne et al., 2009) or modified magmatic and meteoric fluids in the Carajás Fe deposits, Brazil (Figueiredo e Silva et al., 2013).

The study by Rosière and Rios (2004) indicated that the ore-forming processes preceding formation of the final product, i.e. high-grade hematite Fe ore, were also not restricted to a single fluid alteration event affecting a parent BIF. They proposed that in Fe deposits of the Quadrilátero Ferrífero district, Brazil, magnetite mineralization predating the transformation to a high-grade hematite ore, resulted from contraction accompanied by influx of reduced metamorphic fluids and connate water (Rosière and Rios, 2004). Belevtsev et al. (1991) describe epigenetic, magnetite, quartz-absent BIF (52–56% Fe) as a proto-ore for the porous, dispersed-hematite–martite, high-grade Fe ores (60–70% Fe) hosted by the BIF of the Krivoy Rog Belt (KRB). This paper aims to unravel the processes behind the formation of Fe ore precursors generated before the enrichment to the supergene dispersed-hematite–martite, high-grade ores. Fe ore precursors include metamorphosed low-grade Fe ore (31–37% Fe) and iron-rich quartzites (38–45% Fe) as well as compacted, quartz-absent Fe ore (52–56% Fe), which is locally named massive, high-grade ore (Belevtsev et al., 1991). These ore types are actively exploited in the KRB in numerous mines, even at depths exceeding 1.3 km. The rocks of KRB have undergone a very complex evolution with multiple metamorphic, metasomatic and magmatic–hydrothermal events, extensive deformation and supergene alteration (Bobrov et al., 2002). Consequently, the generation of high-grade iron ores in this region is not fully understood. The current genetic model relies on the assumption that contraction and partial BIF leaching by hydrothermal fluids of metamorphic origin were responsible for the hypogene iron ore upgrade to epigenetic, compacted high-grade ore, 52–56% Fe (Belevtsev et al., 1991), however an influence of fluids from other sources has been neither confirmed nor excluded (Lazarenko et al., 1977). Unraveling the fluid evolution within the Fe deposits at Krivoy Rog is crucial to understanding the origin of these ore bodies and could lead to improved genetic models and increased exploration success in the area.

The purpose of this study is to characterize the fluids that formed the iron ores at Krivoy Rog through analysis of fluid inclusions. We use microthermometry and laser Raman techniques on a series of quartz veins and breccias from the low-grade and high-grade iron ores as well as acoustic decrepitometry on ore minerals in order to constrain the composition and source of fluids involved in formation of the iron ores.

2. Geology of the Krivoy Rog Belt

The KRB is situated within the Ukrainian Shield close to the border between two geological units, the Paleoproterozoic Kirovogradskiy terrane and the Archean Middle Dniprean (Dnyepropyetrovskiy) terrane (Bobrov et al., 2002; Yesipchuk et al., 2004) (Fig. 1A). The KRB forms an elongated structure, which is constrained by the deep-seated Krivoy Rog–Kremenchug fault zone to the west and the Saksaganskiy and Demurinskiy granitoid massifs to the east (Fig. 1B). The Mesoarchean age of the Saksaganskiy granitoids is 3.067 ± 0.081 Ga (Yesipchuk et al., 2004; Stepanyuk et al., 2010), however the time span of their formation is unknown. The currently valid stratigraphy of the region and of the Krivoy Rog Belt itself is constantly under debate and requires actualization (Paranko et al., 2005; Khudur, 2006; Paranko et al., 2011).

The KRB hosts the Paleoproterozoic Krivoy Rog Series (equivalent of the Supergroup), which comprises six Suites (corresponding to Groups): the Novokrivorozhskaya Suite, the Skelevatskaya Suite, the metakomatiite rock association, the iron ore-bearing Saksaganskaya Suite, the Gdantsevskaya Suite and the Gleyevatskaya Suite (Figs. 1B, 2a, b) (Bobrov et al., 2002; Yesipchuk et al., 2004). The Krivoy Rog Series is underlain by the oldest metavolcanic rocks of the KRB, the Konkskaya Series (Figs. 1B, 2a, b) (Bobrov et al., 2002).

The Novokrivorozhskaya and Skelevatskaya Suites (Figs. 1B, 2a, b) represent metaconglomerate-schist and metaconglomerate-sandstone–schist rock associations, respectively (Bobrov et al., 2002). The metakomatiite rock association (Figs. 1B, 2a, b) is represented by fissure type rocks, and effusive ultramafic lava flows, which were metamorphosed to talc-carbonate schists (Paranko and Mikhnitskaya, 1991; Paranko, 1993; Paranko et al., 1993; Khudur, 2006; Pieczonka et al., 2011). This suite has a thickness of up to 150 m and extends throughout the entire length of the KRB, yet its origin is still unclear (Paranko and Mikhnitskaya, 1991). Its contact with the Skelevatskaya Suite is gradational, whereas the upper boundary is associated with thrust zones (Paranko and Mikhnitskaya, 1991). The Saksaganskaya Suite (Figs. 1B, 2a, b) of a thickness up to 1500 m (Shcherbak and Bobrov, 2005) comprises seven sets of alternating schist and BIF horizons (Fig. 3) (Bobrov et al., 2002). The former are composed of ferruginous schists and barren quartzites, whereas the latter consist of banded ferruginous quartzites (e. g. silicate–magnetite quartzites, jaspilites, locally containing tiger-eye variety) and high-grade iron ores (Paranko and Mikhnitskaya, 1991; Bobrov et al., 2002) (Fig. 4). In the late Paleoproterozoic the rocks of the Saksaganskaya Suite underwent extensive deformation including folding, faulting, metamorphism, thrusting and metasomatism (Bobrov et al., 2002). The metamorphic grades vary from garnet zone greenschist facies at $T = 430–550$ °C in the central part of the KRB and staurolite-bearing epidote–amphibolite facies at $T = 510–600$ °C in the southern and northern parts of the KRB (Belevtsev et al., 1983, 1991). The Saksaganskaya Suite is unconformably overlain by the Gdantsevskaya Suite (1400 m) and the Gleyevatskaya Suite (1500–2000 m) (Figs. 1B, 2a, b) (Paranko and Mikhnitskaya, 1991; Paranko, 1993, 1997; Bobrov et al., 2002).

The Archean Konkskaya Series and Paleoproterozoic Krivoy Rog Series (Novokrivorozhskaya–Saksaganskaya Suites) dip to the west and form a monoclinal structure, which is crosscut by thrust zones (Kalyayev et al., 1984; Paranko, 1993; Reshetnyak, 1993; Bobrov

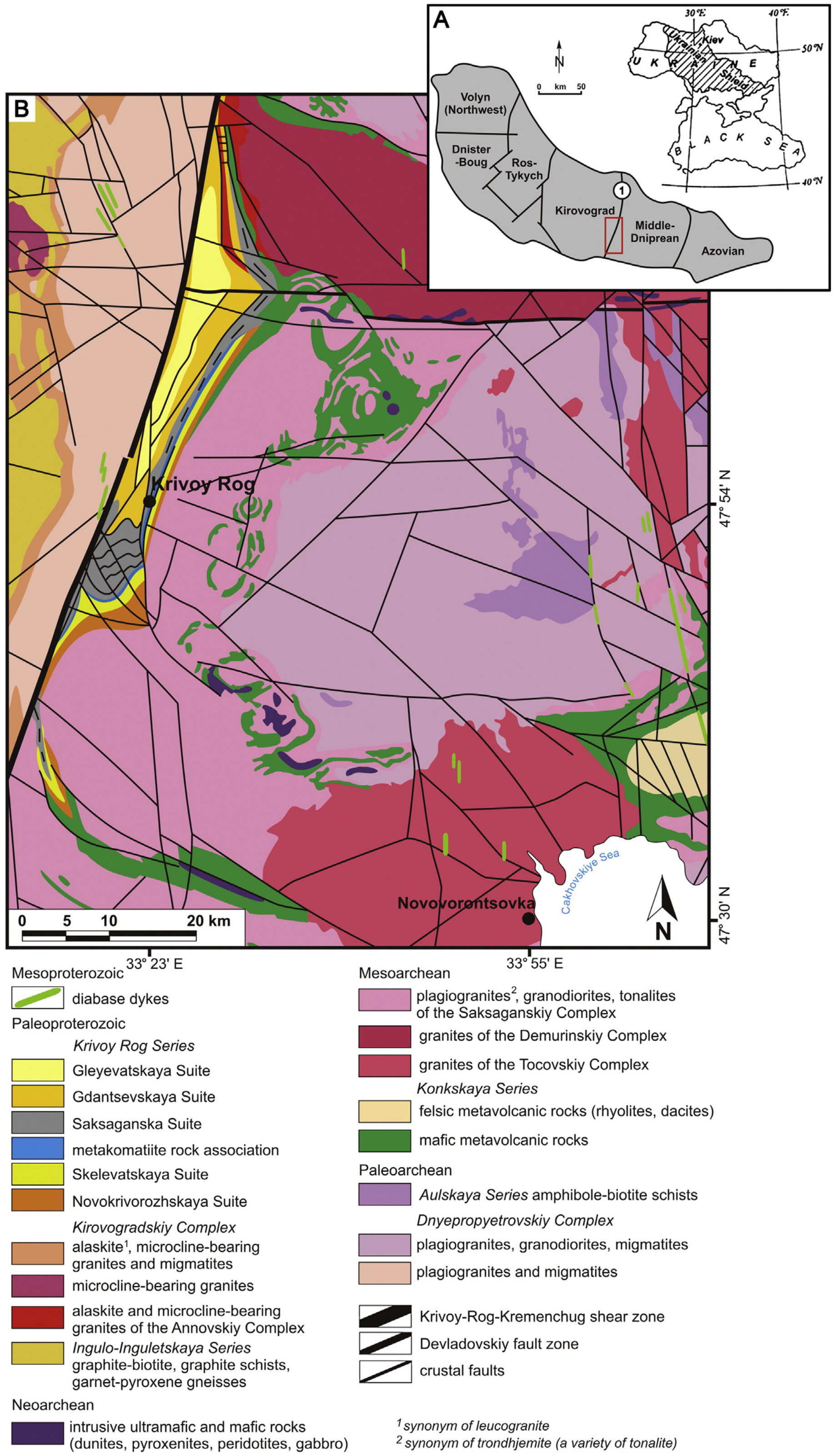

Fig. 1. A—Tectonic provinces of the Ukrainian Shield, 1-Krivoy Rog–Kremenchug megashear (after Bobrov et al., 2002); B—regional geological sketch of crystalline basement of the Ukrainian Shield, Krivoy Rog region (modified, after Paranko et al., 1992).

et al., 2002) (Fig. 2a, b). The Saksaganskiy tectonic block (Fig. 2c), situated in the center of the KRB, is crosscut by the Saksaganskiy thrust zone, which extends its entire length (40 km) (Paranko et al., 1992; Paranko and Butyrin, 2004; Khudur, 2006). The inner structure of the thrust zone is imbricated and consists of thrust slices, which link with each other in a fan-like manner (Khudur, 2006). The thrust surface dips westward and the dip angle decreases with the depth (Fig. 2a).

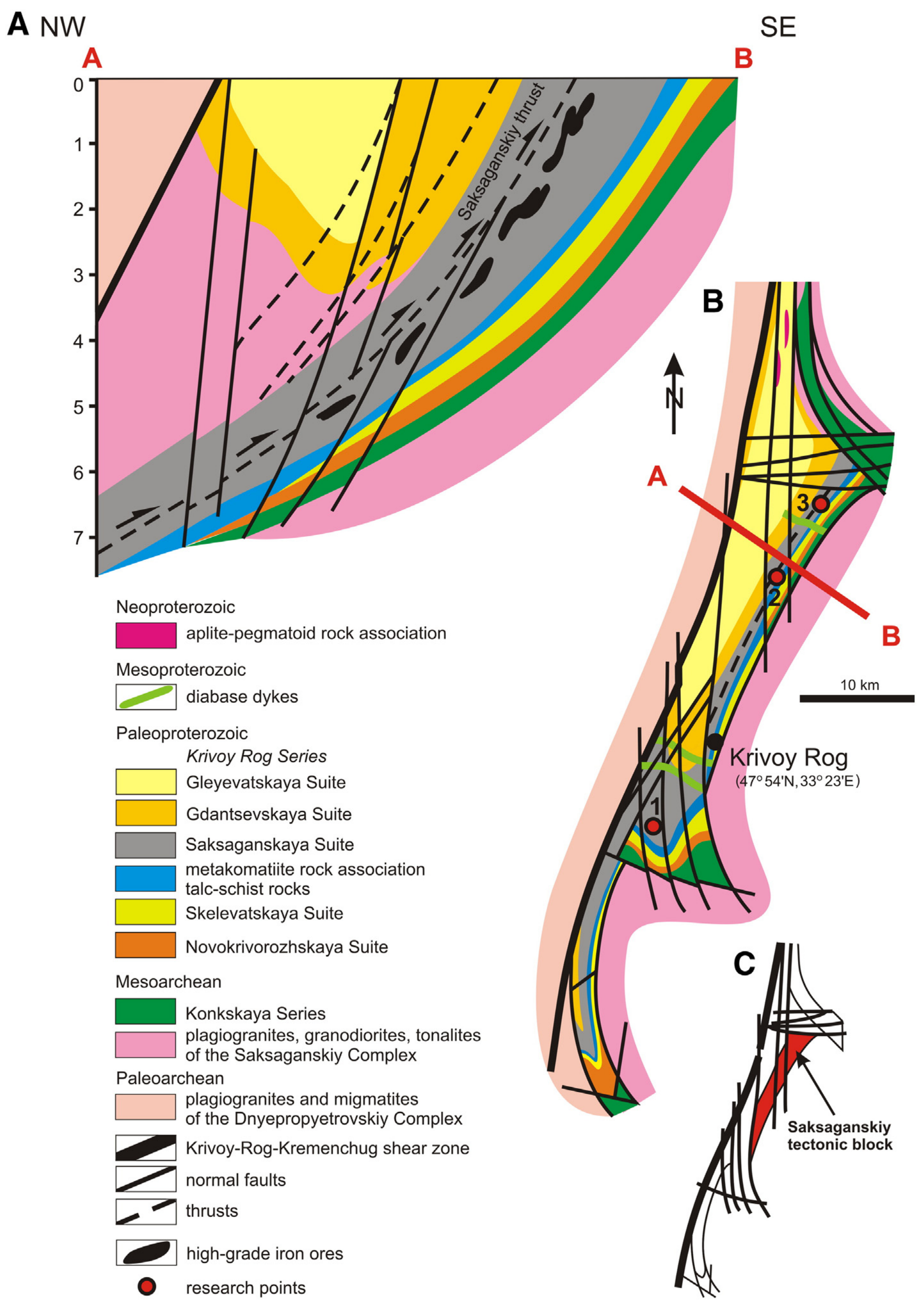

Fig. 2. Geology of the Krivoy Rog Belt (KRB): a—geological cross-section of the central part of the KRB (modified, after Bobrov et al., 2002; Paranko et al., 1992), b—geological map of the KRB (Bobrov et al., 2002), c—tectonic sketch of the KRB (Paranko et al., 1992).

3. Genesis of iron ores

Iron deposits within KRB are confined lithologically to the Saksaganskaya Suite BIF (Belevtsev et al., 1991). The exploited Fe ores are classified based on the Fe content: iron quartzites corresponding to low-grade ores (31–37% Fe), iron-rich quartzites (38–45% Fe) and high-grade ores, which include compacted, massive ores containing ~52–56% of Fe and porous supergene hematite ores comprising up to 60–70% of Fe (Belevtsev et al., 1991). Examples of these ore types are shown in Fig. 4.

3.1. High-grade Fe ores

The Saksaganskiy type, supergene dispersed-hematite–martite high-grade ore (>58% Fe) and epigenetic hypogene, high-grade compacted ores (52–56% Fe) are currently mined underground (e.g. in the Fruzne mine) in the Saksaganskiy ore field (Saksaganskiy tectonic block). These ores comprise deposits associated with a great variety of structures. In the southern part of the Saksaganskiy block they form steeply dipping bodies occurring in zones of intensive folding and faulting, whereas in the northern part of the block they are associated with fold hinges and flexures (Belevtsev et al., 1991). The high-grade ores form lenses, bed-like or columnar ore bodies within the 5th and 6th iron ore horizons (Belevtsev et al., 1991) and their occurrence is restricted to footwalls of thrust zones controlled by talc-carbonate schists (Fig. 2a) (Paranko, 1993; Shcherbak and Bobrov, 2005).

The hypogene, compacted iron ores from the Saksaganskiy ore field comprise two mineralogical varieties: massive quartz–martite ore (52.5–56.3% Fe) and magnetite ore, 52.01–56.5% Fe, av. 54.5% Fe (Belevtsev et al., 1991). These ores are the precursors to globally recognized martite and dispersed-hematite–martite high-grade Fe ores (>58% Fe according to international standards) composed of

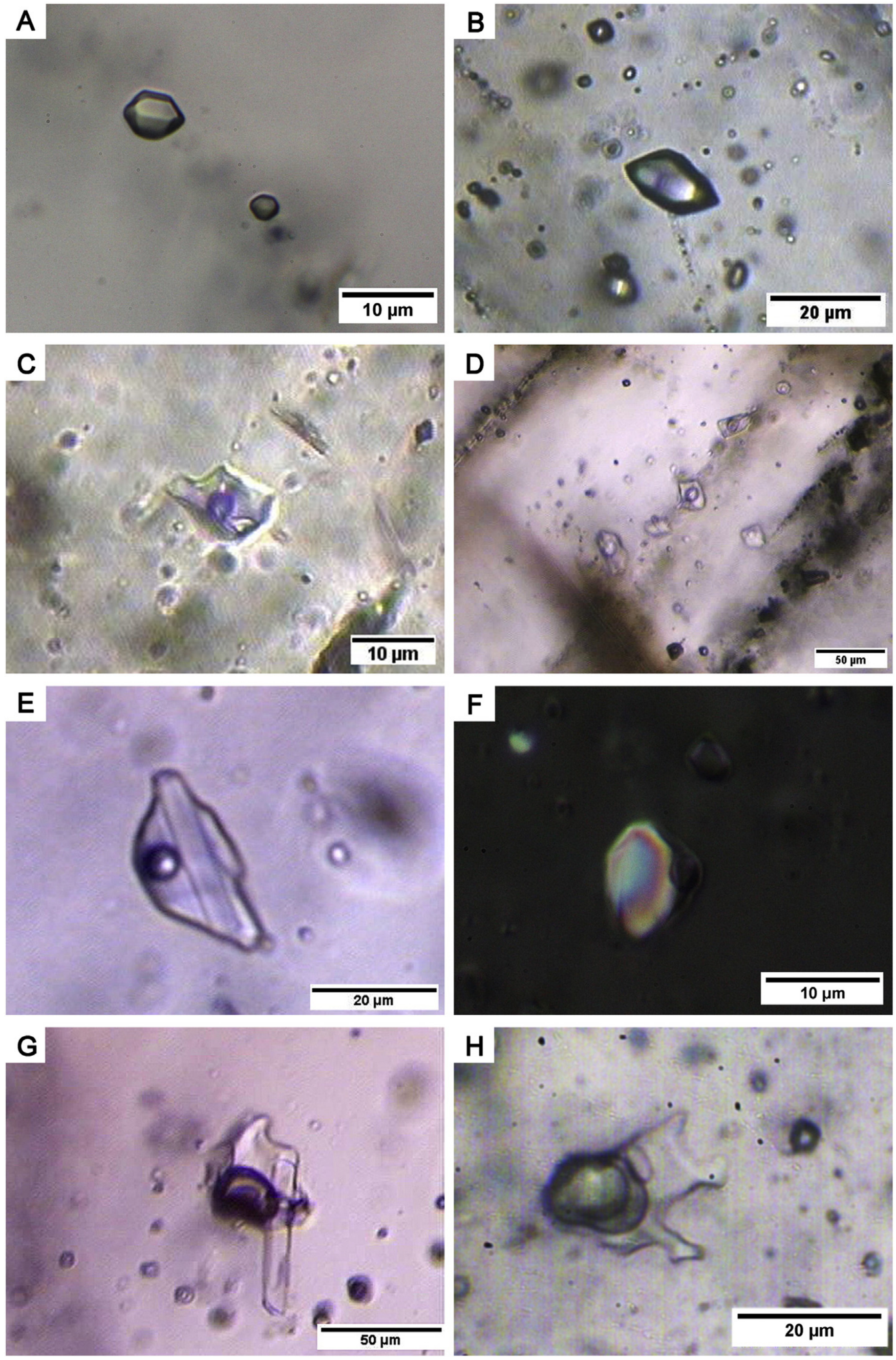

Fig. 6. Fluid inclusion assemblages hosted by quartz vein 1 and vein 2, low-grade iron ore. A—one-phase, liquid, negative crystal shaped, carbonic fluid inclusions (type I), B—one-phase, vapor carbonic fluid inclusion (type I), C—two-phase aqueous fluid inclusion (type II), D—trail of two-phase aqueous-carbonic fluid inclusions (type III), E—a three-phase fluid inclusion (type III) containing an aqueous solution, vapor CO_2 bubble and an engulfed nahcolite crystal, F—a three-phase fluid inclusion (type III) with large birefringent nahcolite occupying almost entire volume of the inclusion (cross-polarized light), G—a three-phase fluid inclusion (type III) comprising an aqueous solution, vapor CO_2 bubble and a nahcolite crystal crosscutting the fluid inclusion wall, H—a four-phase fluid inclusion (type III) containing an aqueous solution, vapor CO_2 surrounded by liquid CO_2 (dark bubbles) and a small nahcolite crystal.

clathrate melting) or were lower than T_m(cla) implying homogenization in the metastable absence of clathrate (Fig. 7A). On the contrary, all fluid inclusions from vein 2 homogenized in the Q_2 conditions (coexistence of the four phases: aqueous liquid, CO_2 vapor, CO_2 liquid, clathrate). CO_2-clathrate melting temperatures below 10 °C in the presence of CO_2 liquid and vapor (i. e. Q_2 melting) indicate the presence of salt in the aqueous phase. It was assumed that the presence of the nahcolite in fluid inclusions had no impact on the measurements due to the petrographical evidence indicating accidental trapping (Fig. 6G) and the random distribution of fluid inclusions with nahcolite on the histogram suggests a lack of relationship between their $T_h(CO_2)$ and the presence of this crystal (Fig. 7A). Densities of the CO_2 phase range between 0.52 and 0.99 g/cm^3, whereas the total densities of fluid inclusions vary between 0.95 and 0.98 g/cm^3. The x(CO_2) values range between 0.03 and 0.36 with a mode value of 0.10. The salinity of the aqueous phase is low and ranges between 2.46 and 7.21 mass% NaCl equiv.

6.1.4. Type IV

Late, two-phase (L + V) aqueous and three-phase (L + L + V) aqueous-carbonic fluid inclusions are flat and large usually exceeding

6.3.2.1. Type 4. The quartz crystal of the matrix contains three different primary fluid inclusions coexisting with each other: two-phase (L + V) aqueous — type 4 (18 μm, $\varphi_{vap} = 0.19$), three-phase aqueous (L + V + S) with a solid phase — type 4 (12 μm) and one-phase carbonic (L) (20 μm) (Fig. 11B). The two-phase, aqueous fluid inclusion (type 4) is irregular in shape and homogenized at $T_h(LV \rightarrow L) = 283$ °C. The density of the fluid within inclusion is 0.94 g/cm^3, whereas the $T_m(ice) = -16.85$ °C (Fig. 10B) indicates a high salinity of 20.11 mass% NaCl equiv. (Fig. 10C). The angular, three-phase fluid inclusion (type 4), containing a cubic crystal, partly homogenized at $T_h(LVS \rightarrow LS) = +130$ °C. Its gas phase is covered by a graphite rim ($T_{cryst} = 525$ °C), whereas the salinity of the aqueous solution (4.87 mass% NaCl equiv.) is significantly lower compared to the salinity of coexisting two-phase inclusion. This fact together with lack of response during Raman analysis suggests that the visible cubic phase (Fig. 11B) is a daughter crystal of halite, which indicates the true salinity of the fluid inclusion of nearly 35 mass% NaCl equiv.

6.3.2.2. Type 5. Quartz clasts contain primary, one-phase (L) fluid inclusions, which are rarely accompanied by several solid inclusions of hematite. The fluid inclusions (7–24 μm) tend to be spherical, cylindrical, cubic or negative crystal shaped (Fig. 11C, D). They were frozen to nucleate a gas bubble at low temperatures and subsequently heated to acquire $T_h(LV \rightarrow L)$ in a range between −46.5 and −35.4 °C corresponding to densities between 1.072 and 1.03 g/cm^3 (Appendices E, F, G). Decreased $T_m(CO_2)$ values, varying between −60.3 and −61.9 °C (Fig. 12), indicate the presence of CH_4 and N_2 (Fig. 9). According to the Raman data the average CH_4/N_2 ratio is 3:1, therefore these fluid inclusions belong to the CO_2–CH_4–N_2 system.

7. Baro-acoustic decrepitation

The analyses of two samples of magnetite from the low-grade iron ore show one major peak, typical for magnetite (Fig. 13). The magnitudes differ significantly, which is probably caused by variations in the abundance or sizes of fluid inclusions. The onset temperatures, generalized for both veins, are around 530 °C.

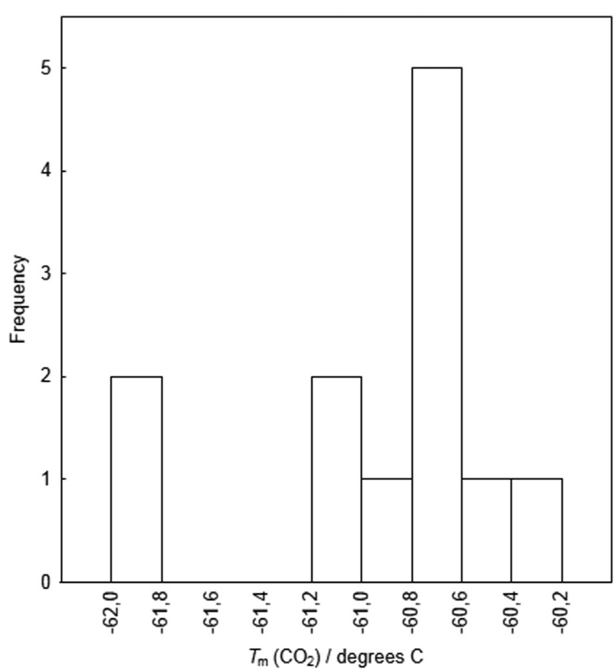

Fig. 12. $T_m(CO_2)$ of one-phase, carbonic fluid inclusions (type 5) hosted by quartz breccia clasts, thrust zone.

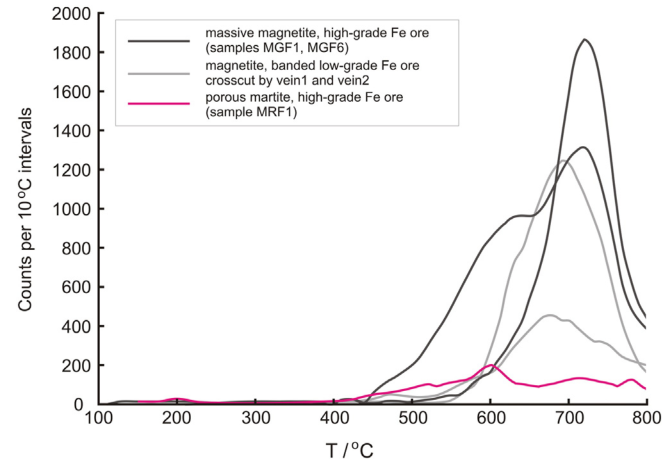

Fig. 13. The results of the baro-acoustic decrepitation of fluid inclusions hosted by ore minerals comprising low-grade iron ore (banded magnetite) from Yugok open pit and high-grade massive magnetite ore and porous martite ore from Frunze underground mine.

Both samples from the high-grade massive, magnetite ore, MGF1 and MGF6 come from the same sampling site but from different specimens. Sample MGF6 comprises almost pure magnetite, whereas sample MGF1 contains thin specular hematite layers alternating with magnetite layers. This slightly differing mineralogy probably affected the decrepitation curves, which show different numbers of peaks as well as the peak intensities (Fig. 13). The main intensity peaks remain in almost the same temperature interval and the onset temperatures range from 430 up to 500 °C.

The porous martite ore (sample MRF1) shows much lower decrepitation intensity compared to the magnetite ores indicating a low abundance of fluid inclusions. Very low decrepitation is observed at the onset temperature around 400 °C (Fig. 13).

All decrepitation curves lack a low-temperature peak around 200 °C, indicating an absence of CO_2-rich fluid inclusions.

8. Interpretation

8.1. Fluid types

Based on the fluid inclusion petrography and compositional data from microthermometry and Raman spectroscopy, quartz veins within the low-grade Fe ore host fluid inclusions representing four types of fluids: carbonic, early and late aqueous and low salinity H_2O–$CO_2(\pm N_2$–$CH_4)$–NaCl($\pm NaHCO_3$). The quartz vein from iron-rich quartzites preserved one distinguishable type of fluid: H_2O–$CO_2(\pm N_2$–$CH_4)$ ± NaCl. Five types of fluids could be distinguished within the thrust zone: CO_2–CH_4–$N_2(\pm C)$, $CO_2(\pm N_2$–$CH_4)$, low salinity H_2O–N_2–CH_4–NaCl, moderate salinity H_2O–N_2–CH_4–NaCl($\pm CO_2$, ±C) and high salinity H_2O–NaCl(±C). Magnetite from the low-grade iron ore and massive, high-grade ore contains fluid inclusions, which represent most probably two different aqueous fluids, however their exact compositions remain unknown. A summary table of fluid inclusion types is included in Appendix H.

Fluid compositions differ depending on the associated iron ore type. Fluids from the thrust zone, which are strictly related to the hypogene high-grade ore mineralization (Paranko, 1993; Pieczonka et al., 2011), are clearly distinct from fluids that circulated within the low-grade iron ore (iron quartzites) and iron-rich quartzites. The highest salinities are characteristic of fluids related to the thrust zone, whereas very low fluid salinities are typical of iron-rich quartzites and the low-grade iron ore. Fluids from the thrust zone are much more enriched in methane compared to those from the low-grade and iron-rich quartzites.

melting of rocks and subsequent igneous and volcanic activity of the Saksaganskiy massif. The magmatic activity of this massif may also be explained by generation of a mantle plume beneath the Dnyepropyetrovskiy terrane, although these hypotheses, both novel for this region, require verification and more research. On the other hand, infiltration of heated basinal brines may also produce fluid inclusions of high salinity (type 4 inclusions). Nevertheless, if the brines were involved, instead of the magmatic–hydrothermal fluids, they required a heat source, e.g. the Saksaganskiy massif, to attain high temperatures (minimum $T_t = 283$ °C). Highly saline, hot brines might have pervasively leached iron from surrounding rocks during upward migration. Fluid inclusions, which trapped ancient meteoric water ($T_h = 115$–195 °C), were documented in supergene quartz from the dispersed-hematite–martite, high-grade ores by Kalinichenko (1992). If these temperatures are not true constraints, the possibility of influence of the fluids from the thrust zone described in this paper on the formation of the dispersed-hematite–martite high-grade ores as well, cannot be neglected.

High-grade, magnetite ores were formed in a temperature range (430–500 °C) suggesting that the iron ore upgrade might have been facilitated by fluid immiscibility and mixing (Fig. 19).

The gas phase of aqueous fluid inclusions, representing H_2O–N_2–CH_4–NaCl and H_2O–N_2–CH_4–NaCl(±CO_2, ±C) fluids, contains admixtures of N_2 prevailing over CH_4 (types 1, 2, 3). The nitrogen may come from the mantle or may be a result of fluid interaction with graphite schists (Fig. 4D) and decomposition of clay minerals in temperatures around 500 °C (Faure and Mensing, 2005). The latter possibility is supported by crystallization temperatures exceeding 500 °C, which were calculated for graphite found within fluid inclusions (types 1, 4, 5). The graphite might have resulted from a reaction of CO_2 with an aqueous solution or it might have precipitated during heating generated perhaps by late, high-temperature fluids.

The carbonic-rich fluid inclusions (type 5 and CO_2-rich type) represent fluids derived from at least two different sources. The CO_2–CH_4–N_2(±C) fluid, preserved as type 5 inclusions, might have been enriched in reduced C during interaction with surrounding rocks, e.g. graphite schists. The fluid evolution suggests a relatively long transport, therefore it might also have been supplied from the deep-seated Krivoy-Rog Kremenchug fault zone. The CO_2(±N_2–CH_4) fluids, represented by CO_2-rich type inclusions, may be associated with metamorphic decarbonation.

9. Implications for the genetic model

9.1. Metamorphic stage

The earlier, metamorphic stage occurred in all localities and affected all rocks of the Krivoy Rog BIF. In this stage, the low-grade iron ore (iron quartzites) and iron-rich quartzites were formed. The low-grade iron ore was progressively metamorphosed at temperatures around 530 °C as indicated by the decrepitation analysis. During this episode, circulating metamorphic fluids precipitated silica to form quartz veins. According to the fluid inclusion analysis vein formation was determined by fluctuating metamorphic conditions, especially a fluctuating pressure. The minimum P–T conditions for the vein formation were $T_{min} = 219$–246 °C and $P_{min} = 130$–158 MPa. The metamorphic fluids showed different densities and typically contained CO_2 and low salinity aqueous solution up to 7.21 mass% NaCl equiv. Four kinds of percolating fluids were distinguished within all types of iron quartzites: CO_2-rich, H_2O, H_2O–CO_2(±N_2–CH_4)–NaCl(±$NaHCO_3$) and H_2O–CO_2(±N_2–CH_4)-NaCl. The origin of nahcolite ($NaHCO_3$) remains unclear. The fluids were derived from metamorphic reactions, dehydration and decarbonation. Decomposition of Fe-bearing carbonates might have played a significant role in the generation of metamorphic magnetite leading to enrichment of barren quartzites to the low-grade Fe ore and iron-rich quartzites.

9.2. Metasomatic stage

The later, metasomatic stage occurred only within the Saksaganskiy tectonic block and was strictly associated with the Saksaganskiy thrust zone.

9.2.1. High-grade Fe ores (Frunze mine)

The porous, martite high-grade ore was formed by supergene oxidation, which removed fluid inclusions during replacement of magnetite by martite. In contrast, the massive magnetite high-grade ore preserved fluid inclusions, which were trapped at temperatures close to 430–500 °C. These temperatures are close to the upper limit of regional metamorphism in the Saksagan region and suggest that fluid inclusions might have preserved a thermal signature other than metamorphic, however more analyses are required to support this suggestion. The fluid composition was not possible to unravel, but it most likely does not contain CO_2. It is proposed that the fluid inclusions may comprise a high salinity aqueous solution. The magnetite high-grade ore, most probably, resulted from fluid alteration of magnetite quartzites.

It is anticipated that the Fe ore upgrade to the magnetite high-grade ores might have involved fluids similar, at least to some degree, to those which are described within the Saksaganskiy thrust zone. This assumption is supported by location of these ores within the 5th ore horizon in the footwall of the thrust zone, restriction to the same tectonic block and also to the presence of the talc-schist horizon encountered within the Frunze mine. However, this mine is situated near the boundary, which divides the Saksaganskiy ore field into northern and southern parts based on differentiation between the structure types hosting the iron ore deposits. The processes which generated the structural variability are not well constrained, therefore it is not clear if they were entirely similar for Fe deposits in the Frunze mine as well as beneath the Balka Severnaya Krasnaya outcrop.

9.2.2. Thrust zone

This study reveals and emphasizes the importance of the multiple fluid flow events in the Saksaganskiy thrust zone. According to the compositional and textural features of fluid inclusions three episodes involving different fluids were distinguished within this zone (Fig. 20). These events were contemporaneous with thrusting and brecciation.

Episode I was dominated by introduction of the CO_2-rich fluids. It involved 3 metamorphic primary fluids of different compositions: CO_2–CH_4–N_2(±C), CO_2(±N_2–CH_4) and low salinity H_2O–N_2–CH_4–NaCl (Fig. 20). The carbonic fluids were probably derived from decomposition of carbonates or/and from deeper sources. Minimum temperatures of the low salinity (6.38–7.1 mass% NaCl equiv.) aqueous fluids were 256–276 °C. Country rocks within the shear zones (e.g. schists) interacted with these fluids supplying them with CH_4 and N_2. An interaction of the CH_4-enriched fluids with hematite might have caused its reduction to magnetite.

During episode II the aqueous fluids H_2O–N_2–CH_4–NaCl(±CO_2, ±C) of moderate salinities (15.22–16.76 mass% NaCl equiv.) were expulsed into the system (Fig. 20). They were most probably of metamorphic origin and their $T_h = 239$–370 °C vary greatly due to re-equilibration. These fluids were N_2-rich and the origin of this component is ambiguous as it might have been derived from the mantle or from country rocks.

Episode III was associated with high salinity (20.11–35.0 mass% NaCl equiv.) H_2O–NaCl(±C) fluids of $T_{min} = 283$ °C (Fig. 20). The fluid inclusion analysis suggests that these fluids resulted from mixing of metamorphic and secondary magmatic fluids or introduction of heated basinal brines.

The aqueous fluids show an increase in salinity from early to late episodes (Fig. 20). This trend supports multiple, incremental input of high salinity fluids into the thrust zone through time. Metamorphic low-salinity, aqueous fluids might have periodically mixed with hot, high salinity magmatic–hydrothermal fluids or heated basinal brines. The

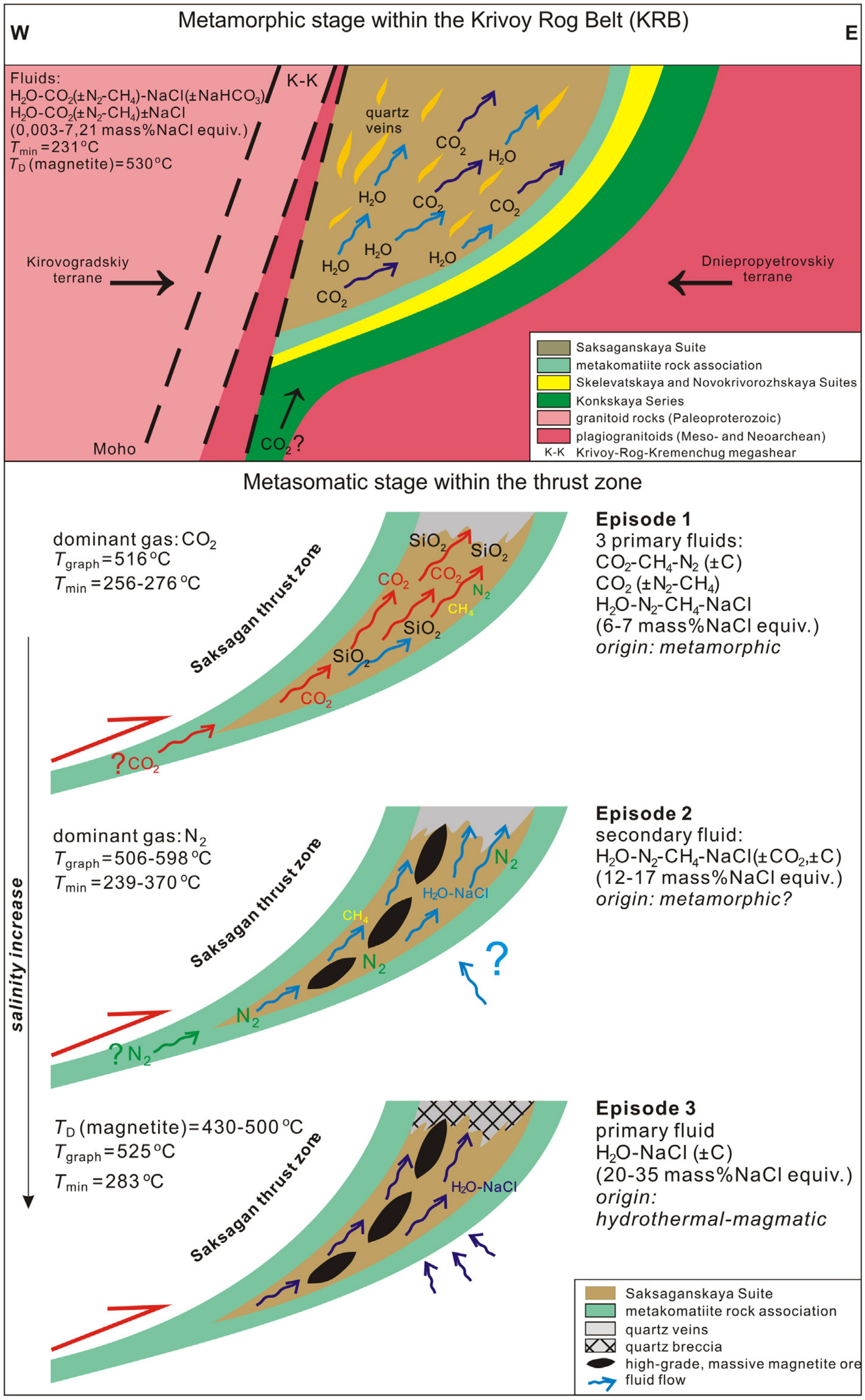

Fig. 20. Schematic illustrations showing metamorphic fluid flow stage within the Krivoy Rog Belt and episodes of multiple fluid flow (metasomatic stage) within thrust zone during the upgrade of iron quartzites (low-grade iron ore and iron-rich quartzites) to massive, high-grade iron ores.

crystallization temperatures of graphite detected in quartz-hosted fluid inclusions exceeded 500 °C. This fact, together with the decrepitation results, may suggest that the iron ore upgrade to high-grade, magnetite ore took place during all episodes at temperatures close to 430–500 °C. The enrichment was facilitated by a complex interaction of BIF with carbonic-rich and low salinity aqueous fluids of metamorphic origin and hot, high salinity fluids, most probably, prior to infiltration of lower temperature meteoric waters responsible for supergene oxidation. The activity of the adjacent Saksaganskiy igneous body, which initiated thrusting, might have been responsible for introduction of the high salinity magmatic–hydrothermal fluids or heating up the basinal brines. These hot, high salinity fluids might have become enriched in iron due to pervasive alteration of the metavolcanic Konkskaya Series or lower iron quartzite horizons of the Krivoy Rog BIF.

10. Concluding remarks

The fluid inclusion study of Fe ores from the Krivoy Rog district revealed that the history of fluid evolution within the Saksaganskiy ore field is more complex compared to the exploitation area of the Skelevatske–Magnetitove deposit, which is located outside this tectonic unit.

The study indicates the structurally controlled, hot, high salinity fluid flow in the vicinity of the high-grade Fe ore bodies in contrast to areas of the low-grade Fe ore exploitation, where this type of fluid was absent. The low-grade iron ores and iron-rich quartzites were not altered by external fluid influx and therefore were prevented from upgrade to the high-grade Fe ores. If the externally derived, high salinity fluid percolated solely within the Saksaganskiy ore field it may be a useful vector to high-grade mineralization at great depths.

More research within the KRB is required in order to verify and fully understand the genetic relationship between the thrust zone, the iron ore enrichment and the high salinity fluids. Identification of the salt types within fluid inclusions and elemental analysis of an aqueous solution could constrain the origin and possible reservoirs of the high salinity fluids and further improve the genetic model. Future research should take into consideration a possible impact of the Saksaganskiy massif as a source of the fluid itself or as a heat source necessary to heat up the infiltrating basinal brines.

Acknowledgments

This article includes the results of PhD research projects undertaken by the main author Marta Sośnicka. It is based on her PhD thesis entitled: "Fluid types and their genetic meaning for the BIF belt formation, Krivoy Rog, Ukraine" at the AGH University of Science and Technology in Cracow, Poland under the supervision of Professor Adam Piestrzyński. This doctoral research benefited from Erasmus Scholarship no. ERAS/44/10-11 at the University of Leoben in Austria (2010/2011), the Dean Grant no. 15.11.140.205 at the Faculty of Geology, Geophysics and Environmental Protection (AGH, 2012) and the Swedish Institute Scholarship no. 382/00096/2012 (Visby Program for PhD studies in Sweden 2013) at Stockholm University in Sweden. MS is truly thankful to supervisor Prof. Adam Piestrzyński and all the people who strongly supported this research. Prof. Steffen Hagemann and Prof. Thomas Angerer are acknowledged for their critical and very insightful reviews.

Appendix A

Microthermometry data of type III fluid inclusions hosted by quartz vein 1 and 2, low-grade iron ore: morphologies, sizes (the longest diameters), presence of nahcolite crystals at 20 °C (nahc), homogenization temperatures of CO_2 phase–$T_h(CO_2)$, melting temperatures of CO_2—clathrate–T_m(cla), and volume fractions of CO_2—$\varphi(CO_2)$ at 20 °C.

Inclusion No.	Morphology	Size (μm)	nahc	T_h (CO_2)/°C	T_m (cla)/°C	$\varphi(CO_2)$
Ink11P1A5-1	cylindrical	30			8	0.16
Ink11P1A5-2	cylindrical, angular	27	+	4.5	8.3	0.14
Ink11P1A5-3	spherical	18		9	8.1	0.19
Ink11P1A5-4	cylindrical	13		8.5	8.3	0.25
Ink11P1A5-5	spherical	18	+	15	8.4	0.13
Ink11P1A5-6	negative crystal shaped	18		30.5	8.5	0.25
Ink11P1A1-1	negative crystal shaped	21		7	8.4	0.16
Ink11P1A1-2	negative crystal shaped	18		6.7	8.1	0.18
Ink11P1A1-3	cubical	16		6.9	8.3	0.13
Ink11P1A3-1	spherical	22		30	7.9	0.26
Ink11P1A3-2	cylindrical	59		-3.7	7.8	0.16
Ink11P1A3-3	negative crystal shaped	13			8.4	0.22
Ink11P1A6-1	negative crystal shaped	19		-0.1	7.9	0.17
Ink11P1A6-2	cylindrical, angular	23		2.7	7.8	0.16
Ink11P1A6-3	cubical	24		13.9	8.6	0.22
Ink11P1A4-1	cylindrical, angular	32			7.6	0.37
Ink11P1A4-2	spherical	28			8.1	0.68
Ink11P1A4-3	spherical	19			6	0.48
Ink11P1A7-1	spherical, angular	18		9.8	8.2	0.15
Ink11P1A7-2	cubical	21	+			0.28
Ink11P1A7-3	irregular	43			7.3	0.43
Ink11P1A7-4	spherical	12		12	8.3	0.14
Ink11P1A8-1	negative crystal shaped	15			8.2	0.31
Ink11P1A8-2	cylindrical, angular	12			8.1	0.17
Ink11P3A1-1	cylindrical	91	+			0.13
Ink11P3A1-2	negative crystal shaped	38		8.2	8.3	0.19
Ink11P3A1-3	spherical	21		10.6	8.3	0.28
Ink11P3A1-4	cylindrical, angular	39		7.6	8.4	0.15
Ink11P3A1-5	spherical, angular	30	+	28	8.3	0.17
Ink11P3A1-6	spherical	33		12.3	8	0.22
Ink11P3A1-7	negative crystal shaped	14		11.6	8.3	0.28
Ink11P3A1-8	spherical	20		12.1	8.3	0.19
Ink11P3A1-9	spherical	24		10.9	8.2	0.28
Ink11P3A1-10	spherical, angular	20	+	-1.3	8.2	0.16
Ink11P3A1-11	spherical, angular	17		25	8.2	0.25
Ink11P4A1-1	spherical, angular	31		-5.9	7.8	0.60
Ink11P4A1-2	cylindrical	24		-3.5	8.1	0.19
Ink11P4A1-3	cubical	15	+			0.15
Ink11P4A1-4	cubical	16		23	8.2	0.21
Ink11P4A1-5	irregular, angular	14				0.08
Ink11P4A2-1	irregular	28		10	8.1	0.51
Ink11P4A2-2	negative crystal shaped	17		10	8.1	0.42
Ink11P4A2-3	cylindrical, angular	29	+	2.8	8.1	0.15
Ink11P4A2-4	cylindrical	16		1.5	8.1	0.19
Ink11P4A3-1	irregular	28		-8	8.1	0.14
Ink11P4A3-2	irregular	16		-5.5	8.1	0.20
Ink11P4A3-3	negative crystal shaped	18		-10.4	8.2	0.15
K1F1-1	cylindrical	115	+	11.2	7.8	0.17
K1F1-2	irregular, angular	17	+			0.11
K1F1-3	cubical, angular	38		15	7	0.22
K1F1-4	spherical, angular	16		22.2	6.9	0.37
K1F1-5	cylindrical	26		11.8	7	0.22
K1F1-6	irregular	42		15.1	7.7	0.14
K1F1-7	spherical	29	+		7.9	0.07
K1FS-1	cylindrical	50		31	7.7	0.13
K1F2-8	irregular	45	+	23	7.7	0.19
K1F3-9	cylindrical	35	+	27.8	8.2	0.31
K1FI-10	irregular	68			8.2	0.18
K1F3-1	negative crystal shaped	61	+	21.8	7.9	0.20
K1F3-2	spherical	51		19.7	8	0.15
K1F3-3	spherical	27		17.5	8	0.24
K1F3-4	cylindrical	44	+			0.10
K1F3-5	spherical, angular	19				0.20
K1F3-6	cylindrical	32			7.9	0.35
K1F4-7	spherical, angular	58		27.5	7.6	0.17
K1F4-8	cylindrical	47		25	7.7	0.18
K1F4-9	negative crystal shaped	35		23.7	7.7	0.28
K1F4-10	spherical, angular	28		20.2	7.7	0.18
K1F4-11	cylindrical	25		18.5	7.8	0.20
K1F4-12	spherical	47		31	7.8	0.11
K1F5-13	negative crystal shaped	72		12.8	8	0.31
K1F5-14	cylindrical	64		16.3	7.7	0.25
K1F5-15	negative crystal shaped	49		14.7	7.7	0.22
K1F5-16	negative crystal shaped	26		14.6	7.7	0.28
K1FSR-1	irregular	73				0.26
K1F6-1	spherical	55	+	23.1	7.5	0.19
K1F6-2	irregular	62		20.5	7.8	0.18
K1F6-3	cubical, angular	49	+	30	7.7	0.19
K1F6-4	spherical, angular	27		22.1	7.6	0.18
K1F6-5	cylindrical, angular	38		22.2	7.7	0.19
K1F6-6	irregular	37		17.9	7.5	0.18
K1F6-7	cylindrical, angular	39		19.1	7.7	0.26
K1F6-8	cylindrical, angular	42		15.9	7.8	0.18
K1F7-1	spherical	43			8.2	0.15